Ocean Modelling 120 (2017) 27–40

Contents lists available at ScienceDirect

Ocean Modelling

journal homepage: www.elsevier.com/locate/ocemod

Kinetic energy flux budget across air-sea interface

Yalin Fan[a,*], Paul Hwang[b]

[a] Oceanography Division, Naval Research Laboratory, Stennis Space Center, MS 39529, United States
[b] Remote Sensing Division, Naval Research Laboratory, Washington, DC, United States

ARTICLE INFO

Keywords:
Air-sea interaction
Turbulent kinetic energy flux
Ocean surface gravity waves
Wave modeling

ABSTRACT

The kinetic energy (KE) fluxes into subsurface currents (EF_c) is an important boundary condition for ocean circulation models. Traditionally, numerical models assume the KE flux from wind (EF_{air}) is identical to EF_c, that is, no net KE is gained (or lost) by surface waves. This assumption, however, is invalid when the surface wave field is not fully developed, and acquires KE when it grows in space or time. In this study, numerical experiments are performed to investigate the KE flux budget across the air-sea interface under both uniform and idealized tropical cyclone (TC) winds. The wave fields are simulated using the WAVEWATCH III model under different wind forcing. The difference between EF_{air} and EF_c is estimated using an air-sea KE budget model. To address the uncertainty of these estimates resides in the variation of source functions, two source function packages are used for this study: the ST4 source package (Ardhuin et al, 2010), and the ST6 source package (Babanin, 2011). The modeled EF_c is significantly reduced relative to EF_{air} under growing seas for both the uniform and TC experiments. The reduction can be as large as 20%, and the variation of this ratio is highly dependent on the choice of source function for the wave model. Normalized EF_c are found to be consistent with analytical expressions by Hwang and Sletten (2008) and Hwang and Walsh (2016) and field observations by Terray et al. (1996) and Drennan et al. (1996), while the scatters are more widely in the TC cases due to the complexity of the associated wave field. The waves may even give up KE to subsurface currents in the left rear quadrant of fast moving storms. Our results also suggest that the normalized KE fluxes may depend on both wave age and friction velocity (u_*).

1. Introduction

The kinetic energy (KE) flux from surface waves to ocean currents (EF_c) is responsible for the enhancement of the near surface turbulent kinetic energy (TKE) dissipation rate (e.g., Terray et al., 1996). Prediction of EF_c is not only essential for estimating bubble and sea spray generation, air-sea gas exchange, and other air-sea interaction processes, but also of great importance in determining both transfer rates across the air-sea interface to the mixed layer below and the evolution of the mixed layer itself.

EF_c is an important boundary condition for the turbulent closure models used to represent the small-scale turbulence in the oceanic boundary layer that cannot be resolved by the ocean models, such as the popularly used Mellor-Yamada level 2.5 closure (Mellor and Yamada, 1982). Turbulent closure models usually solve the TKE equation to obtain eddy viscosity (K) and eddy diffusivity for buoyancy (K_B) and energy (K_E):

$$\frac{\partial TKE}{\partial t} = \frac{\partial}{\partial z}\left(K_E \frac{\partial TKE}{\partial z}\right) + K\frac{\partial U}{\partial z}\frac{\partial U}{\partial z} + K_B\frac{\partial B}{\partial z} - \varepsilon \quad (1)$$

where the net flux of TKE at the ocean surface (z = 0) is given as $K_E\frac{\partial TKE}{\partial z} = EF_c$. Eq. (1) is only presented here to illustrate the importance of EF_c in turbulent closure models. The details of this equation including all terms, boundary conditions, and choice of parameters can be found in Noh and Kim (1999).

As important as EF_c is, it is often forgotten because, traditionally, numerical models assume the KE flux from wind (EF_{air}) is identical to EF_c and parameterize it using the friction velocity u_* as mu_*^3, where m is an empirical constant (Noh and Kim, 1999). Fully coupled models such as the Unified Wave Interface-Coupled Model (UWIN-CM) developed by University of Miami (Chen and Curcic, 2016; Curcic et al., 2016) that utilized UMWM (an efficient wave model to provide fully atmosphere-wave-ocean coupling in hurricane forecast systems, Donelan et al., 2012) and the Navy's Coupled Ocean Atmosphere Mesoscale Prediction System – Tropical Cyclone (COAMPS-TC, Smith et al., 2013) have explicitly taken into account of the wind-wave and wave-current momentum fluxes, but no special attentions have been given on the energy flux.

The assumption of EF_c equals to EF_{air} is invalid when the surface wave field is not fully developed. When surface waves propagate, they

* Corresponding author.
E-mail addresses: yalin.fan@nrlssc.navy.m, yalin.fan@nrlssc.navy.mil (Y. Fan).

http://dx.doi.org/10.1016/j.ocemod.2017.10.010
Received 11 April 2017; Received in revised form 17 October 2017; Accepted 24 October 2017
1463-5003/ Published by Elsevier Ltd.

transport energy in the wave propagation direction. When waves grow (decay) in time, they extract more (less) KE from air than they give up to the subsurface currents. If the surface wave field is not homogeneous, the divergence of these fluxes will also contribute to the difference between EF_{air} and EF_c. Therefore, both spatial and temporal evolutions of the wave field need to be taken into account for accurate estimation of EF_c. This is especially true under tropical cyclone (TC) conditions where the surface wave field is complex and fast varying in space and time and may significantly affect the energy flux from wind into ocean.

Additionally, transfer of momentum and energy can occur both up and down in that swells can interact with the airflow and create wave-driven winds (Harris, 1966). Donelan et al. (1997) measured the air-sea momentum flux via eddy correlation off the coast of Virginia and found that swell aligned with the wind can deliver momentum to the atmosphere. When this happens, the momentum and KE flux to the ocean will be reduced consequently. In this study, we found that this negative flux is very small compare to the air input (less than 1%) in all our experiments and it can be neglected in the budget calculation.

Ocean wave modeling is a very useful and convenient way to obtain the spatial and temporal distribution of directional wave spectra without the limitations associated with measurements, although the model output may differ from observations because of uncertainties in wind input, model physics, and numeric. During the past 4 decades, considerable improvements have been made in predicting ocean wave directional spectra. Third generation wave models (e.g., WAVEWATCH III (Tolman, 1998), the Wave Model (WAM; Hasselmann et al., 1988), and Simulating Waves Nearshore (SWAN; Booij et al., 1999)) have been used to study surface wave responses during hurricanes, and the modeled wave parameters (significant wave height, mean/dominant wave length, mean/dominant wave direction) are shown to compare well with observations (Phadke et al., 2003; Moon et al., 2003; Xu et al., 2007; Fan et al., 2009b; Allard et al., 2014; Fan and Rogers, 2016). Fully coupled atmosphere-wave-ocean model is suggested for accurate hurricane predictions as well as the corresponding ocean responses (Chen et al., 2007, 2013; Fan et al., 2009a; Liu et al., 2011). Thus, it is essential to understand the behavior of the wave model generated KE flux, which is an important forcing for ocean circulation models, under different wind conditions.

The main objective of this paper is to investigate the effect of surface gravity waves on the KE transfer budget across the air-sea interface under moderate to high wind conditions. In particular, we focus on the difference between the KE fluxes from wind and those into currents by explicitly calculating the KE gained (or lost) due to the spatial and time variation in the surface waves. WAVEWATCH III (WWIII) is used to generate the wave fields for all the calculations.

An uncertainty in these estimates resides in the variation of source functions. Field measurements by Powell et al. (2003) and laboratory work by Donelan et al. (2004) and Takagaki (2012) have suggested that the drag coefficient flattens or even decreases with wind speed at high winds. Takagaki et al. (2016a, b) found in their tank experiments that the distinctive breaking of wind waves is the causes of the saturation of drag coefficients at strong wind speeds. Hence, several modifications to the source functions are implemented in WWIII to reflect such behavior. Liu et al. (2017) compared the performance of four different source function packages within the WWIII framework through intensive comparisons with radar altimeter measurements, scanning radar altimeter measurements, and buoy observations during hurricane Ivan in 2004. Source package ST3 (Janssen, 1991, 2004; Bidlot et al., 2007), ST4 (Ardhuin et al., 2010) and ST6 (Babanin, 2011; Rogers et al., 2012; Zieger et al., 2015) are found to give the most accurate results within the four. ST4 is adapted from Janssen (1991) and Bidlot et al. (2005, 2007) with a reduction of u_* (hence drag coefficient) implemented through reducing the wind input for high frequencies and high winds and allow a balance with a saturation-based dissipation. ST6 is developed based on Donelan et al. (2006) with constraints on the wind input from air-flow separation, wave steepness, and wave breaking. In this study, both source packages are used to calculate the KE gained or lost due to the spatial and time variation in the surface waves and to illustrate the uncertainty brought about by the variation of source functions.

The outline of this paper is as follows. The relation between the fluxes from wind, EF_{air}, and fluxes to currents, EF_c, are formulated in Section 2; a brief outline of the experimental design is introduced in Section 3; the air-sea budget calculation results using the ST4 source function are analyzed in Section 4; Section 5 discusses the uncertainty of the budget calculation due to different source functions using ST6 for illustration; A summary of the major results of this study and concluding remarks are presented in Section 6.

2. Wave spectrum and KE flux budget

Consider a two-dimensional system of orthogonal Cartesian coordinates with x increasing eastward, and y increasing northward. We are concerned with the air-sea KE fluxes influenced by surface gravity waves that are characterized by a wave spectrum $\psi(\omega, \theta)$, where ω is the wave angular frequency and θ is the wave direction. The ocean is assumed to be very deep ($k|D| >> 1$, where k is the wave number, and D is the water depth), therefore surface waves are not influenced by the ocean bottom. This assumption implies the deep water dispersion relation, $\omega^2 = gk$. We will focus our analysis on ocean areas away from the boundaries without concerns of any boundary effects.

WWIII version 4.18 (Tolman et al., 2014) is used to simulate the evolution of wave spectra for all experiments. The model explicitly accounts for wind input, wave-wave interaction, and dissipation due to whitecapping and wave-bottom interaction, and solves the spectral action density balance equation for directional wavenumber spectra. In this study, the wave spectrum in WWIII is calculated in 24 directions. In each direction, the spectrum is discretized using 40 frequencies extending from $f = 0.0285$ to 1.1726 Hz (wave length of 1.1–1920 m) with a logarithmic increment of $f_{n+1} = 1.1f_n$, where f_n is the nth frequency. The diagnostic tail, proportional to f^{-5}, is imposed at a cutoff frequency that is equal to 10 times of the mean frequency. Since the kinetic energy in the wave field is dominated by large waves near the peak, the effect of different spectra tail parameterization on KE is negligible and not investigated in this study.

The differences between the KE fluxes from wind and those into subsurface currents are estimated by explicitly calculating the KE gained or lost due to the spatial and time variation in the surface waves.

The total energy (E) contained in the wave field is obtained from the complete wave spectrum $\psi(\omega, \theta)$ as

$$E = \iint \rho_w g \psi(\omega, \theta) \cdot d\theta \cdot d\omega, \tag{2}$$

where ρ_w is the density of water. The horizontal fluxes of E are obtained as

$$EF_x = \iint \rho_w g C_g(\omega, \theta) \psi(\omega, \theta) \cos\theta \cdot d\theta \cdot d\omega, \tag{3}$$

$$EF_y = \iint \rho_w g C_g(\omega, \theta) \psi(\omega, \theta) \sin\theta \cdot d\theta \cdot d\omega, \tag{4}$$

where EF_x and EF_y are the total wave energy flux in the x and y directions, respectively, and C_g is the group velocity of the waves. Then, KE flux budget can be given as:

$$EF_{air} = EF_c + \left(\frac{\partial EF_x}{\partial x} + \frac{\partial EF_y}{\partial y} \right) + \frac{\partial E}{\partial t}, \tag{5}$$

On the right-hand side in Eq. (5), the term in the parentheses is the horizontal divergence of KE flux in the wave field, and the last term is the local time derivative of KE in waves, that is, KE gained (lost) by growing (decaying) waves.

3. Experimental design

The air-sea flux budget is investigated in a series of numerical experiments. We consider both steady uniform wind and tropical cyclone wind problems following the experimental design of Fan et al. (2010). Despite the complicated temporal and spatial distributions of the hurricane wind field, many analyses of wind and wave measurements under hurricane conditions have shown that fetch- and duration-limited wave growth functions derived from steady wind forcing conditions are applicable to the wave fields generated by hurricanes (Young, 1988, 1998, 2003, 2006; Young and Vinoth, 2013; Hwang, 2016; Hwang and Walsh, 2016; Hwang and Fan, 2017). Thus, the fetch and duration dependent experiments can help us gain basic and clear understanding of the kinetic energy variations with different wind speed before we get into complicated hurricane wind conditions.

The water depth is set to be 4000 m for the whole model domain in all experiments of this study so that the surface gravity waves have no interaction with the bottom.

3.1. Steady uniform wind experiments

Both duration and fetch-dependent experiments are conducted under steady uniform wind from 10 to 50 ms^{-1} with an increment of 10 ms^{-1}. The model domain is set up to be 10° by 40° in the latitude and longitude directions with 1/12° resolution for the fetch-dependent experiments (Fig. 1a), and 10° by 60° in the latitude and longitude directions with 1/3° resolution for the duration-dependent experiments (Fig. 1b). Spatially uniform eastward wind is applied over the entire model domain for all experiments. In the fetch-dependent experiments, surface wave spectrum is obtained along the middle cross-section of the model domain after 72 h of the model integration when the wave field becomes practically steady. For the duration-dependent experiments, we analyze the surface wave spectrum at a grid point 5° from the south boundary and 55° from the west boundary for the first 72 h of model integration. According to Fan et al. (2010), the wave field becomes fetch-dependent after about 78 h at this location when the wind speed is 50 ms^{-1}, the first 72 h represents a pure duration dependent problem. The effect of the model boundaries is negligible in all experiments and the wave fields remain spatially homogenous during the first 72 h around the chosen grid points.

Fan et al. (2010) have shown that "the wave fields simulated with WWIII appear to have the same growth relation with fetch compared with Donelan et al. (1992) but slightly slower with fetch than Hasselmann et al. (1973). The normalized significant wave height in the model simulations (in both the time and fetch dependent experiments) is related to the wave age with the same power law as in the observations.". Their finding gives us confidence in using the WWIII spectra for energy flux budget study.

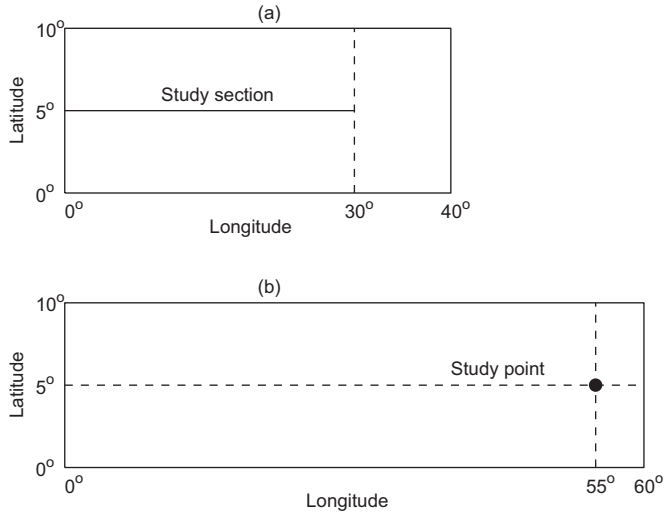

Fig. 1. Domain configuration for (a) the fetch-dependent experiments and (b) the duration-dependent experiments. Uniform wind will blow from west to east over the entire model domain for all experiments. Modified from Fig. 2 in Fan et al. (2010).

Table 1
Experimental designs of the TC experiments. Here, TSP, MWS and RMW denote translation speed of the TC, maximum wind speed and radius of maximum winds, respectively.

Experiment	TC type	TSP (ms^{-1})	MWS (ms^{-1})	RMW (km)
A	Axisymmetric, stationary	0	45	50, 60, 70, 80, 90
B	Axisymmetric, stationary	0	35, 45, 55	70
C	Axisymmetric, moving	5, 10	45	70
D	Asymmetric, moving	5, 10	45	70

3.2. Tropical cyclone experiments

The Holland (1980) analytical model is used to prescribe the axisymmetric wind field in the tropical cyclone (TC) experiments with given input parameters of the central and ambient pressure, the maximum wind speed (MWS), and the radius of maximum wind speed (RMW). Four sets of experiments are conducted to study how the air-sea energy flux budget is affect by changes in the TC parameters (Table 1): Stationary TC Exp. A varies the RMW from 50 km to 90 km with a fixed MWS of 45 ms^{-1}; in stationary TC Exp. B the MWS varies from 35 ms^{-1} to 55 ms^{-1} with a fixed RMW of 70 km; the effect of different TC translation speed (TSP) is investigated in Exp. C by moving the axisymmetric TC with a constant TSP of 5 ms^{-1} and 10 ms^{-1}; and finally the effect of asymmetric wind structure is investigated in Exp. D by adding half of the translation speed to the axisymmetric wind field. In all experiments, we set the ambient and central pressure to 1012 hPa and 968 hPa respectively.

A square model domain of 10° × 10° is used for all stationary TC experiments, and a rectangle domain of 18° × 30° in the longitude and latitude direction is used for the moving TC experiments. In all experiments, the grid increment is 1/12° in both directions and the time increment is 100 s. All results are presented after a spin-up time of 54 h, when a quasi-steady state is achieved. In the case of a moving TC a quasi-steady state is achieved relative to the TC center.

The "input wave age" $c_{pi}/u_* = g/(2\pi f_{pi} u_*)$, defined in Moon et al. (2004), is used in the TC experiments instead of the traditional wave age because it represents the state of growth of wind waves relative to local wind forcing. Here f_{pi} is the peak frequency of the wind sea (waves directly forced by wind) estimated using the formulation described in Tolman and Chalikov (1996). Detailed characteristics of wave parameters (significant wave height, wave direction, and input wave age) under stationary and moving TCs are given in Fan et al. (2010).

4. Energy flux budget in growing and complex seas

The air-sea budget calculation results using the ST4 source package are analyzed in this section. In all experiments, EF_{air} is calculated through the integration of the model input source function in all frequencies and directions and EF_c is calculated using Eqs. (2)–(5).

4.1. Steady uniform wind experiments

The normalized KE fluxes plotted against the distance/time (left panels) and wave age (right panels) display similar behaviors in the fetch (Fig. 2) and duration (Fig. 3) dependent experiments. The KE fluxes normalized in terms of the 10-m wind ($\frac{EF_{air}}{\rho_{air}|U10|^3}$ and $\frac{EF_c}{\rho_{air}|U10|^3}$)

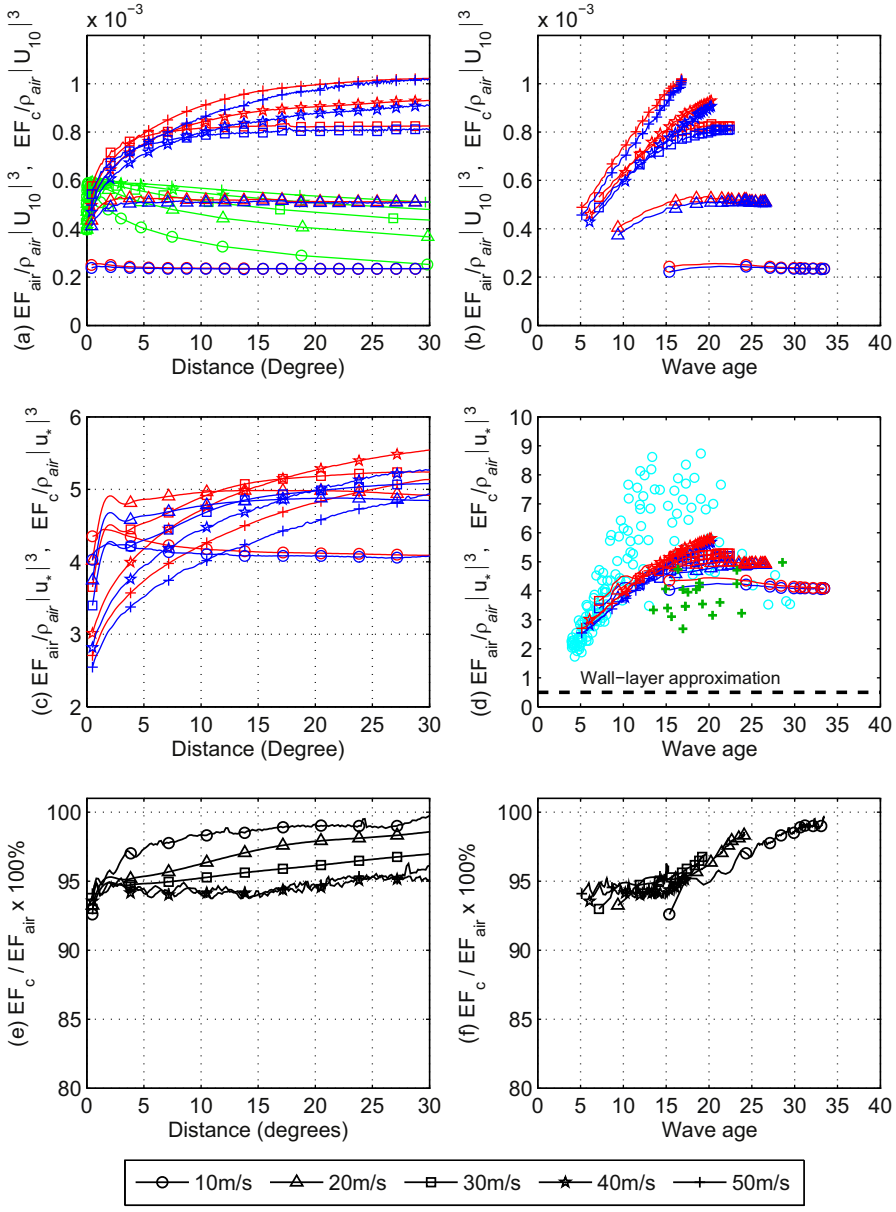

Fig. 2. Kinetic energy flux in the fetch-dependent experiments with steady homogenous winds of 10, 20, 30, 40, and 50 ms^{-1} represented by different symbols in the legend. Upper panels: EF_{air} (red) and EF_c (blue) normalized by 10-m wind speed vs. (a) distance and (b) wave age. In (a), analytical expressions of the normalized EF_c by Hwang and Sletten (2008) (green line with symbols) are given for comparison. Middle panels: EF_{air} (red) and EF_c (blue) normalized by friction velocity vs. (c) distance and (d) wave age. In (d), the wall-layer approximation (black dashed line), data from Drennan et al. (1996) (green cross) and data from Fig. 8 in Terray et al. (1996) (cyan circles) are given for reference. Lower panels: the ratio EF_c/EF_{air} vs. (e) distance and (f) wave age. (For interpretation of the references to color in this figure legend, the reader is referred to the web version of this article.)

increase with wind speed, and the amount of increase significantly reduces for higher wind speed. The difference between the KE flux from air and that into currents is significant when the wave field is growing in time or space, and gradually reduces towards fully developed seas. That is the younger the wave is, the more energy flux the wave extracts from the wind. The magnitude of $\frac{EF_c}{\rho_{air}|U10|^3}$ and its increasing trend with wind speed is consistent with the analytical expression proposed by Hwang and Sletten (2008) given in Figs. 2a and 3a. Notice that the increasing speed of $\frac{EF_c}{\rho_{air}|U10|^3}$ with wind speed in the analytical solution also significantly reduces for high wind speed, similar to what we observe in the model results. Since their parameterization is based on the ensemble mean of a few different wind input functions, the authors suggest that the accuracy of their estimates is roughly within a factor of two (their Fig. 1b), which agrees nicely with the range of our model results.

Unlike the normalized KE fluxes, the ratio of EF_c to EF_{air} are very different between the fetch and duration dependent cases. While the KE flux into currents can become as low as 85% of the flux from air in the duration dependent case (Fig. 3e and f), this ratio is around 95% and higher for the fetch dependent case (Fig. 2e and f). This suggests that the spatial variation induced wave growth is much weaker than the wave growth in time. Also notice that when plotted against wave age, the ratios of EF_c to EF_{air} collapse together for all wind speeds and they increase slowly with wave age in the fetch dependent case. While in the duration dependent case, the ratios increase rapidly with wave age, the higher the wind speed, the faster the increase.

The normalized KE fluxes in terms of the friction velocity u_* ($\frac{EF_{air}}{\rho_{air}|u_*|^3}$ and $\frac{EF_c}{\rho_{air}|u_*|^3}$) vs. wave age are shown in Fig. 2d (3d) for the fetch (duration) dependent problems. Note that these fluxes are much less dependent on the wind speed, compared to the normalized KE fluxes in terms of the 10-m wind speed. It is instructive to compare these fluxes with those obtained from the wall-layer theory (Csanady, 2001) that estimates the KE flux into the current (EF_c) as τ_{air} U_d, where U_d is the surface drift current. This expression assumes that the KE flux only arises from the direct action of the wind stresses τ_{air} on the surface drift current. Based on Wu's (1975) estimate of the surface drift current, $U_d = u_*/2$, the KE flux into currents is then ρ_{air} $u_*^3/2$ (black dashed line), which is significantly smaller than EF_c calculated in our experiments (blue lines with blue symbols).

Our results are generally consistent with previous estimates by

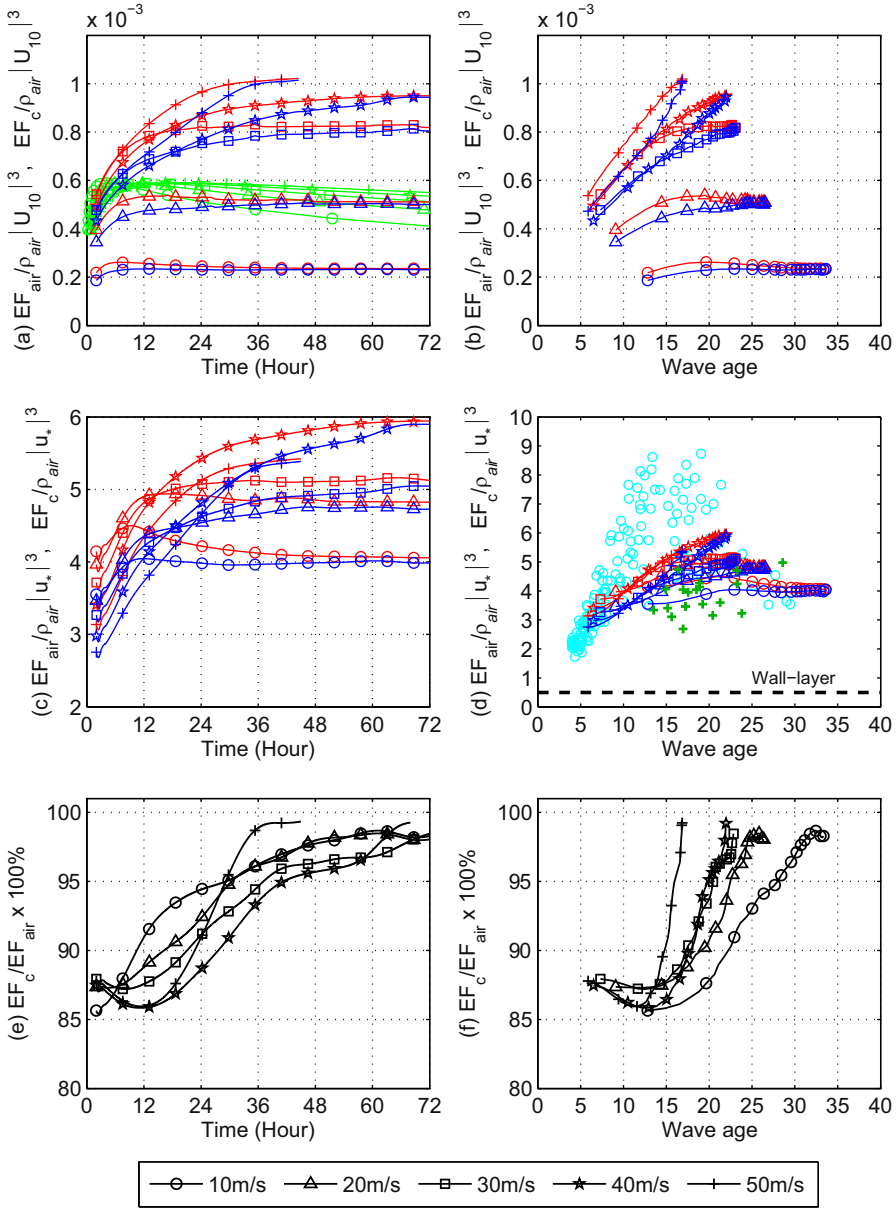

Fig. 3. Kinetic energy flux in the time-dependent experiments with steady homogenous winds of 10, 20, 30, 40, and 50 ms^{-1} represented by different symbols in the legend. Upper panels: EF_{air} (red) and EF_c (blue) normalized by 10-m wind speed vs. (a) time and (b) wave age. In (a), analytical expressions of the normalized EF_c by Hwang and Sletten (2008) (green line with symbols) are given for comparison. Middle panels: EF_{air} (red) and EF_c (blue) normalized by friction velocity vs. (c) time and (d) wave age. In (d), the wall-layer approximation (black dashed line), data from Drennan et al. (1996) (green cross) and data from Fig. 8 in Terray et al. (1996) (cyan circles) are given for reference. Lower panels: the ratio EF_c/EF_{air} vs. (e) time and (f) wave age. (For interpretation of the references to color in this figure legend, the reader is referred to the web version of this article.)

Terray et al. (1996) (cyan circles) and Drennan et al. (1996) (Green crosses). Terray et al. (1996) estimated the KE flux from wind to waves (EF_{air}) by integrating (in ω and in θ) the product of the growth rate, β (by Donelan and Pierson, 1987) and the observed wave spectra (their own data as well as those from Donelan et al., 1985; Kahma, 1981; Hasselmann et al., 1973; and Birch and Ewing, 1986) over a wind speed range of 5 ms^{-1}–22 ms^{-1}. Their $\bar{\varepsilon}/u_*$ is equivalent to our definition of $\frac{EF_{air}}{\rho_{air}|u_*|^3}$ rather than $\frac{EF_c}{\rho_{air}|u_*|^3}$, since they did not account for the flux budget. Drennan et al. (1996) estimated the KE flux in the same manner but using the data obtained during the Surface Waves Dynamics Experiment (SWADE) that took place off the east coast of the United States (Weller et al., 1991). We should note that the majority of the data used in Terray et al. (1996) comes from fetch limited conditions while Drennan et al. (1996) used open ocean data.

One immediately notices large scatter of the previous estimates at intermediate wave ages around 15 with the normalized KE flux varies from 3 to 9 (Figs. 2d and 3d). The estimates by Drennan et al. (1996) are generally lower, possibly because the data were obtained in open ocean conditions. Another likely reason of the large scatter is the normalization of the KE flux by the cube of the friction velocity. A small uncertainty of the friction velocity may cause large variability of the normalized flux. Our numerical results of $\frac{EF_{air}}{\rho_{air}|u_*|^3}$ (red solid lines in Figs. 2d and 3d) agrees very well with Terray et al. (1996) at young wage (less than 10), and are within the scatter of their estimates at higher wave age. It's interesting to notice that our model results for 10 ms^{-1} is lower than the estimates by Terray et al. (1996) and went right through the middle of the estimates by Drennan et al. (1996). This is more likely because the set up of our model experiments are analogue to open ocean conditions where Drennan et al. (1996) conducted their measurements at similar wind speed.

The model results also indicate that the wave age dependence of the KE fluxes varies with wind speed when wave age is greater than 15. At 10 ms^{-1} wind speed, the normalized KE flux is almost independent of the wave age. At higher wind speeds, its rate increase with wave age increases with wind speed. This suggests that the normalized KE flux may not only be a function of wave age, but also a function of wind speed (or u_*).

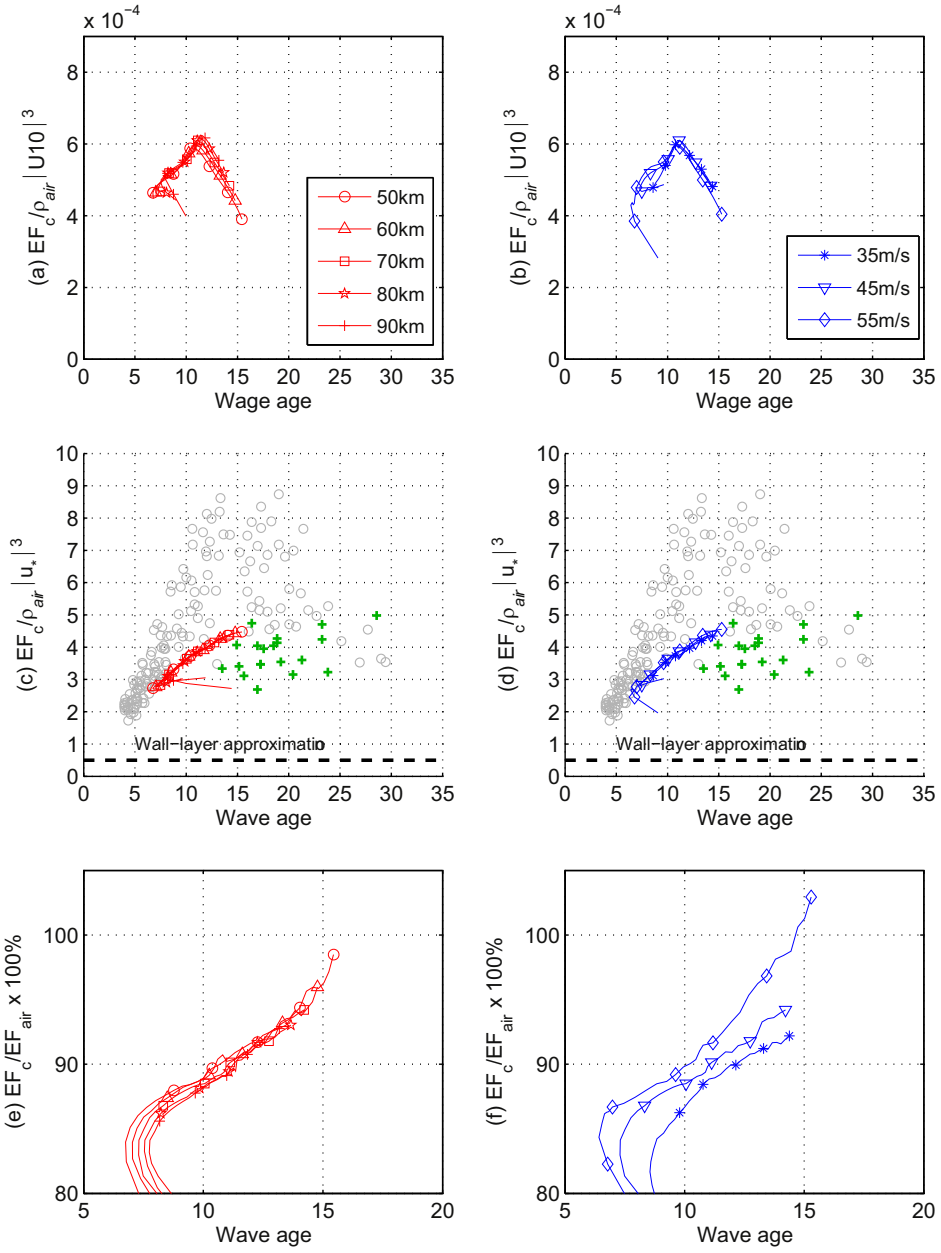

Fig. 4. Normalized kinetic energy flux vs. wave age in the stationary hurricane experiments: Left panels show varies RMS of 50, 60, 70, 80, and 90 km represented by different symbols; Right panels show varies MWS of 35, 45, and 55 ms^{-1} represented by different symbols. Upper panels are EF_c normalized by 10-m wind speed. Middle panels are EF_c normalized by friction velocity, the wall-layer approximation (black dashed line), data from Drennan et al. (1996) (green cross) and data from Fig. 8 in Terray et al. (1996) (gray circles in back ground) are given for reference. Lower panels are the ratio EF_c/EF_{air}. (For interpretation of the references to color in this figure legend, the reader is referred to the web version of this article.)

4.2. TC experiments

4.2.1. Stationary TC

Because both the wind field and the wave field are axisymmetric in all stationary TC experiments (Fan et al., 2010), we analyze the results along one of the radii. In the following figures, we present the results of the normalized KE flux into the currents ($\frac{EF_c}{\rho_{air}|U10|^3}$, $\frac{EF_c}{\rho_{air}|u_*|^3}$), and the ratio EF_c/EF_{air}.

Fig. 4 shows the results of Exp. A (left) and B (right) against input wave age. Only the data within 3° of the storm center is presented here. Since the swells generated near the eyewall will propagate toward the periphery and interact with the air flow above to generate upward energy flux, the magnitude of this upward flux may exceed 1% of the air input beyond 3° from the storm center (not shown) and have notable effect on the estimations of EF_c based Eqs. (2)–(5). There are no results shown close to the center either because the spatial resolution of our model is not sufficient to resolve the wave field in this region. As noted by Fan et al. (2010), the wind radial profiles relative to the normalized distance are practically independent of the RMW within the RMW in the Holland TC wind model, and only slightly different at the storm periphery; while the wind profile significantly varies with the MWS if the pressure difference is kept constant: as the MWS increases, the wind speed decreases more rapidly outside of the RMW.

It is interesting to notice that the normalized KE fluxes, both by 10-m wind ($\frac{EF_c}{\rho_{air}|U10|^3}$) and the friction velocity ($\frac{EF_c}{\rho_{air}|u_*|^3}$), collapse together for all different RMW in experiment A (Fig. 4a and c) and all different MWS in experiment B (Fig. 4b and d). The maximum values of $\frac{EF_c}{\rho_{air}|U10|^3}$ for both experiments are found around the eye wall where the waves are the youngest, and decrease rapidly with wave age for both experiments.

The normalized KE flux by u_*, $\frac{EF_c}{\rho_{air}|u_*|^3}$, are very similar between experiment A and B and within the scatter of previous estimates by Terray et al. (1996) and Drennan et al. (1996). The maximum appears around wave age 15, same as Terray et al. (1996) and then decrease toward lower wave ages.

The ratio of EF_c relative to EF_{air} does not vary with RMW and it increases almost quadratically with wave age. The stronger the storm

intensity, the faster the increase. The main physical mechanism of the smaller KE flux into subsurface currents relative to the wind input is due to the horizontal divergence of the KE flux by surface waves. Since the angle between the dominant wave propagation direction and the wind direction increases with the distance from the center and become more radial direction (Fan et al., 2010), the radial component of the wave KE flux increases with the distance as a function of the wind-wave angle. The radial gradient of this KE flux is always positive, thus the KE flux to subsurface currents is always reduced relative to the flux from wind.

For the experiment with MWS equals to 55 ms^{-1}, EF_c /EF_{air} exceeds 100% at wave age ~15 towards the periphery of the storm. This is because with the larger MWS, the wind speed and hence the significant wave height decreases more rapidly towards the periphery (Fan et al., 2010). Even though the wave direction becomes more radial towards the periphery, the radial component of the wave energy flux ceases to increase and even decreases near the periphery. This suggests that waves that are generated near the eye wall of a very strong TC give up energy to the subsurface currents when they decay farther away from the storm center.

4.2.2. Moving TC

The KE flux budget under axisymmetric moving TCs is investigated in Exp. C with the storm moving northward at a constant speed. In order to minimize the effect of upward energy flux on the estimation of EF_c as discussed earlier in Section 4.2.1, we will only analyze the results of EF_c within 2° of the storm center. As Hwang and Walsh (2016) has pointed out based on their analysis of hurricane Bonnie 1998 wave spectra measurements that "Inside the circle of maximum wind speed, $r < r_m = 74$ km, local wind waves remain dominant to about 50 km; farther inward, the swell contribution increases steadily, particularly in the front quarter". In order to minimize the swell contamination, the areas within 50 km of the hurricane eye is also blocked out from the analysis.

When the storm moves, the waves in the front-right quadrant of the storm track are higher and longer due to the resonance effect caused by the movement of the TC, while those in the rear-left quadrant are lower and shorter (Fan et al., 2010; Hwang and Fan, 2017). As the TSP increases, the wave height and length differences between the front-right and rear-left quadrants increases and the input wave age increases to the right of the TC track as well (Fig. 5a). This is because when the TSP approaches or exceeds the group velocity of the dominant waves (between 8 and 10 ms^{-1}), the waves become "trapped" within the TC and thus produce the higher and older seas.

The spatial distribution of the normalized KE flux $\frac{EF_c}{\rho_{air}|u_*|^3}$ (Fig. 5b) roughly follows the spatial distribution of input wave age and increases towards the periphery to the right and behind the hurricane. The lowest values are found within a short distance to the hurricane center and mainly in the left quadrant (within 2 radius of maximum wind) and immediately behind the eye. It is interesting to notice that there is a large normalized KE flux area wrapped in the minimum normalized KE flux region right along the eye wall in front of the hurricane center, and the values are more profound for the faster moving hurricane. The waves appear to be old in this region, and are surrounded by young waves. The strong divergence in the wave field here can lead to enhanced energy flux into the ocean current by these older waves given up energy and decay in the faster moving hurricane case (Fig. 5b, TSP = 10 ms^{-1}). Also notice that the normalized KE flux $\frac{EF_c}{\rho_{air}|u_*|^3}$ is the smallest right behind the TC center where the youngest waves are generated with the input wave age of 3–5 in both cases.

While the spatial distribution of EF_c is largely controlled by the symmetric wind forcing, it is also influenced by the asymmetric wave field. This asymmetry is more apparent in the faster moving TC case. Unlike the momentum flux whose major reduction due to the wave effects appears in the rear-right quadrant of the TC (Fan et al., 2010), the KE flux reduction by surface waves is most significant (i.e., less KE flux is passed to the currents) in the front-right quadrant. This is because the energy in the wave field is dominated by the spectra peak and thus the maximum energy reduction is found in the same region where the waves are the highest with the sharpest change (both spatial and temporal) of the wave energy, while the calculation of the momentum flux is strongly dependent on the spectral tail which seems to have its sharpest gradient in the right-rear quadrant of the storm. The maximum reduction for the 5 ms^{-1} storm is around the RMW to the right of the TC track (Fig. 5c), and this maximum reduction area is moved further away from the eyewall in the faster moving storm due to the increased asymmetry in the wave field. The KE flux into subsurface currents is more than 15% less than the air input in the right front quadrant of the storm. It is interesting to notice that the waves give up KE back to subsurface currents ($EF_c/EF_{air} > 100\%$) in the left rear quadrant of the faster moving TC indicating that waves that are generated near the eye wall of a faster moving TC give up energy to the subsurface currents when they decay farther away from the storm center.

The scatter plot of $\frac{EF_{air}}{\rho_{air}|u_*|^3}$ and $\frac{EF_c}{\rho_{air}|u_*|^3}$ vs. the wave age are plotted in Fig. 6. $\frac{EF_{air}}{\rho_{air}|u_*|^3}$ is plotted for all the grid points in the entire model domain except the boundary points, while $\frac{EF_c}{\rho_{air}|u_*|^3}$ is only plotted within 2° of the storm center. The color scale shows the magnitude of u_* at each point. Both normalized fluxes show very similar magnitude and variation with wave age compared with the stationary TC cases. The normalized air input ($\frac{EF_{air}}{\rho_{air}|u_*|^3}$) agrees very well with Terray et al. (1996) both in magnitude and trend when the waves are young (wave age less than ~10) and forced by very strong winds, and become lower than their estimates at higher age under weaker winds and consistent with the estimates by Drennan et al. (1996) based on open ocean observations. The maximum normalized fluxes in both experiments are found around wave age 15 and decrease towards younger/older seas, consistent with the estimates by Terray et al. (1996). At lower friction velocities, $\frac{EF_{air}}{\rho_{air}|u_*|^3}$ scatters more widely due to the large variation in the wave field caused by their relative location to the storm center. $\frac{EF_c}{\rho_{air}|u_*|^3}$ is in general consistently lower than $\frac{EF_{air}}{\rho_{air}|u_*|^3}$ at young wave age and under high winds.

Hwang and Walsh (2016) derived an empirical parameterization of the air-sea energy and momentum (MF_{air}) fluxes and apply to a set of hurricane hunter measurements:

$$EF_{air} = 0.20\omega_{\#}^{3.3}\eta_{\#}\rho_a U_{10}^3 \tag{6}$$

$$\frac{MF_{air}}{EF_{air}} = (\omega_p/g)\frac{a+3}{a+4}, \quad -4 < a \le -5 \tag{7}$$

where a is spectral slope, $\omega_{\#} = \omega_p U_{10} g^{-1}$ and $\eta_{\#} = \eta_{rms}^2 g^2 U_{10}^{-4}$ are the dimensionless parameters with ω_p, η_{rms}, and U_{10} being the peak frequency, root mean square (rms) wave elevation, and 10-m wind speed. The friction velocity u_* can be obtained by $u_* = \sqrt{MF_{air}/\rho_{air}}$. Given $a + 3/a + 4$ can be any value equals to 2 or larger for the given a range, the normalized energy flux covers a large range of magnitude. Since the scatter of $\frac{EF_c}{\rho_{air}|u_*|^3}$ and $\frac{EF_{air}}{\rho_{air}|u_*|^3}$ at young wave age under high winds are small and their trends are very similar, it is practical to use the normalized energy flux derived from Eq. (6) and (7) to represent $\frac{EF_c}{\rho_{air}|u_*|^3}$. A reasonably good fit is given by the black line in Fig. 6 when $a + 3/a + 4$ equals to 2.75 is used ($a = -4.57$). The two green lines are given to illustrate the range of the normalized flux with $a + 3/a + 4$ equals to 2 (4) for the upper (lower) line, corresponding to $a = -5$ (-4.33). It is interesting that field observations of the spectral slopes in hurricane and non-hurricane conditions show a normal distribution with mean and standard distribution of -4.48 and 0.53, respectively (Hwang et al., 2017).

In all previous experiments, the wind fields are assumed to be axisymmetric. However, when a TC moves, actual wind speed to the right

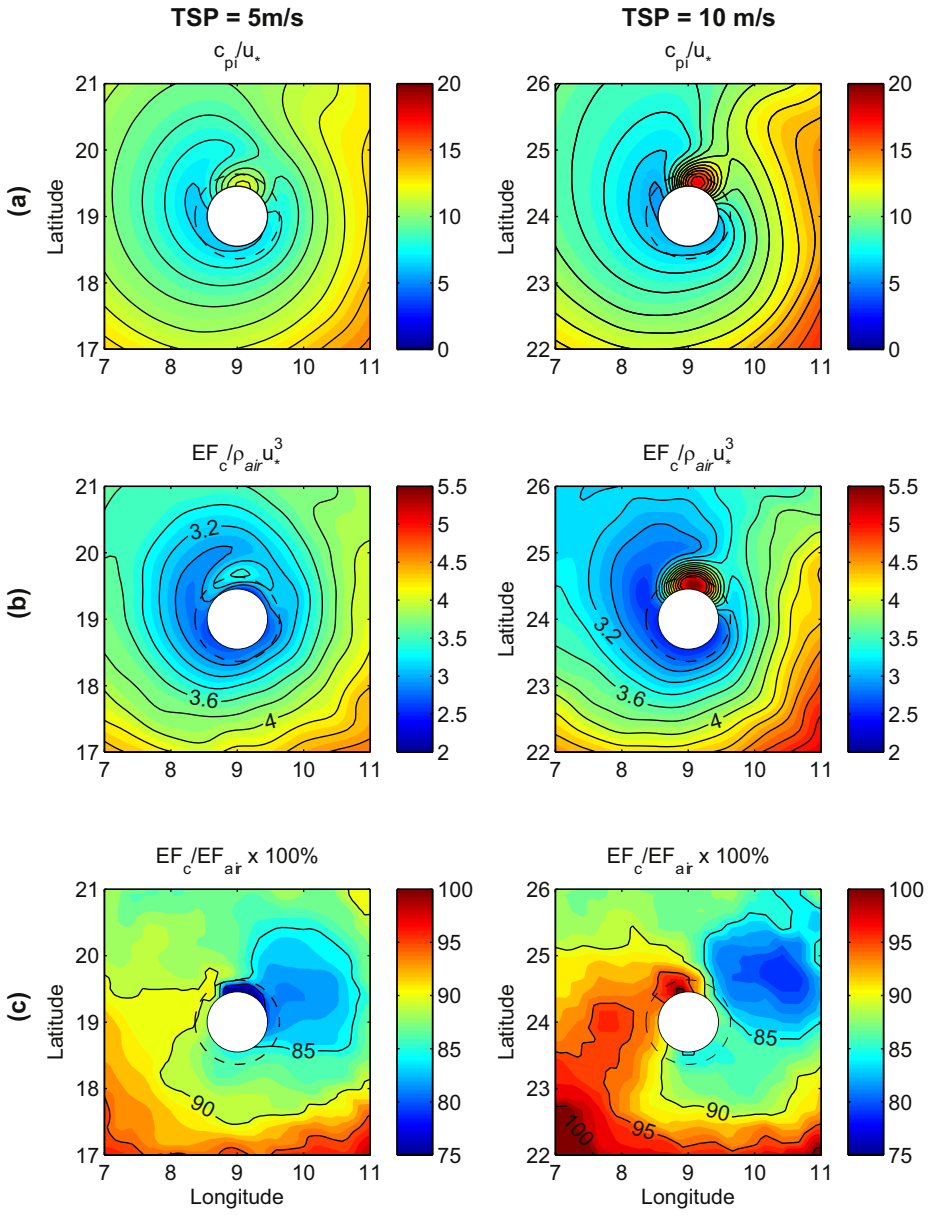

Fig. 5. (a) Input wave age, (b) KE flux into currents normalized by the friction velocity, and (c) the ratio of EF_c/EF_{air} for moving TCs with TSP = 5 ms^{-1} (left) and 10 ms^{-1} (right) heading northward. The dashed circle represent the RMW. 50 km within the center of the TC was blocked out by the white area to eliminate swell effect.

(left) of its track becomes higher (lower) because of addition (subtraction) of the translation speed to the wind speed that is determined by the TC pressure field. The maximum wind speed is therefore usually found in the right-hand side of the TC. However, such asymmetry of the wind field does not make any qualitative changes in the flux budgets when investigated in Exp. D in which we add half of the TC translation speed to the symmetric wind field produced by the Holland model (Table 1).

5. Uncertainty of energy flux budget due to the choice of source functions

Since the wave energy spectrum computed by the wave models is from a balance between input and dissipation, the estimated KE flux budget will apparently depend on the source/dissipation functions we chose for our model. Furthermore, the variation in source function/drag parameterization will also change the normalized fluxes by friction velocity and thus affect the results presented in Section 4.

The least understood aspect of the physics of wave evolution is the dissipation source function. Hasselmann (1974) consider that white capping is the main cause for the dissipation process and it is local in space, whereas Phillips (1985) argues that wave dissipation is rather local in wavenumber space. This is followed by Jenkins (1987) who advocated the picture that breaking waves will generate ocean eddies (turbulence) that will damp the waves. During the next two to three decades, several dissipation source functions have been proposed and widely used in third generation wave models such as Komen et al. (1984) and Tolman and Chalikov (1996). However, these parameterizations were adjusted to close the wave energy balance instead of using the quantitative relationship with observed features. Banner and Young (1994) and Banner et al. (2000, 2002) are the first ones that analyzed breaking in relationship to the formation and instabilities of groups. Following their work, Babanin et al. (2001, 2007a), and Ardhuin et al. (2010) worked on the physics of the process analyzing both laboratory and open-field data. As Cavaleri (2009) has pointed out, “These efforts led to new insights into the process of whitecapping, in a way making even more evident the limits associated with the various parameterizations in use.” Ardhuin et al. (2010) is the first to implement these findings into an operational wave model (WWIII, ST4) through a dissipation function without any prescribed spectral shape

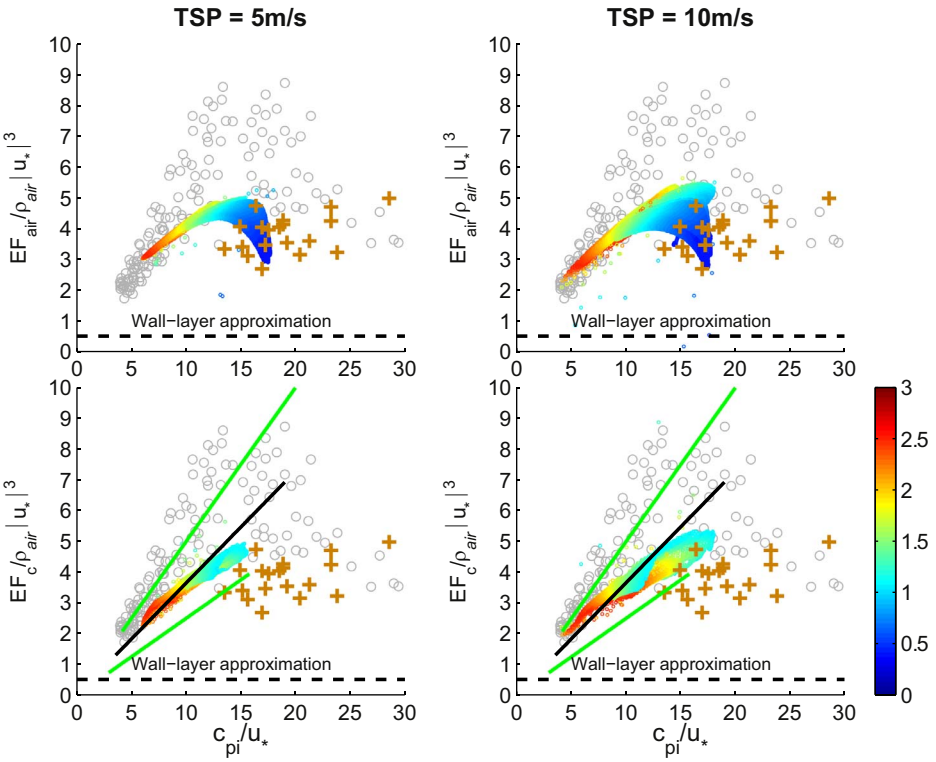

Fig. 6. Scatter plots of the normalized KE flux from the air (top) and that into the ocean currents (bottom) by the friction velocity as a function of the input wave age with translation speed (TSP) of 5 ms^{-1} on the left and 10 ms^{-1} on the right. $\frac{EF_{air}}{\rho_{air}|u_*|^3}$ is plotted at all grid points in the domain while $\frac{EF_c}{\rho_{air}|u_*|^3}$ is only plotted at grid points within 2° of the storm center The color scale shows u_* at each data point. Data from Fig. 8 in Terray et al. (1996) are given for reference by the gray circles. Drennan et al. (1996) estimates are also shown for reference by the brown crosses. The black curve shows $\frac{EF_{air}}{\rho_{air}|u_*|^3}$ computed using Eq. (6) and (7) when set $a + 3/a + 4 = 2.75$. The two green lines are given to illustrate the range of the normalized flux with $a + 3/a + 4$ equals to 2 and 4 for the upper and lower line. (For interpretation of the references to color in this figure legend, the reader is referred to the web version of this article.)

but based on the empirical knowledge of the breaking of random waves from previous researches and the dissipation of swells over long distances due to air friction. Their work is immediately followed by Babanin (2011) and Zieger et al. (2015) who implemented the ST6 package in WWIII that argues the swell attenuation is due to the interaction with ocean turbulence, and thus swells will transfer energy into the ocean when they dissipate rather than to the air.

Because wind input and deep water dissipation functions are tightly coupled and play the important role of closing the energy balance, the evolutional variation of the dissipation term is accompanied by the corresponding modification of the wind input function. In WWIII, the S_{in} and S_{ds} are grouped in packages with switches ST1, ST2, ST3, ST4, ST6, and SLN. For more detail, please see Sections 2.3.6–2.3.11 in Tolman et al. (2014).

In essence, as noted by Tolman et al. (2013): "There is still no universal consensus for S_{in}, and several proposed forms for this are being evaluated as part of the overall effort [of the NOPP operational wave improvement project]. These include the Miles–Janssen form modified for sheltering in the spectral tail region (Banner et al., 2010), and an observation-based form proposed by Donelan et al. (2006) and Babanin et al. (2007b). The potentially strong influence of wave steepness in reducing the growth rate (Peirson and Garcia, 2008) presents an additional element that requires investigation."

In this section, we assess the effect of source package choice on our normalized KE fluxes. The ST6 source package implemented in WWIII is used in the uniform wind and moving TC experiments to illustrate this uncertainty.

5.1. Uniform wind experiments

The results for the uniform wind experiments are plotted in Figs. 7 and 8 in the same manner as Figs. 2 and 3 for easy comparison. The first thing we notice is the very different behavior of the normalized EF_{air} and EF_c for high winds at 40 and 50 ms^{-1}. At low to moderate winds (10–30 ms^{-1}), the normalized KE flux by U_{10} increase with U_{10} for both the fetch and duration dependent experiments (Figs. 7a, b and 8 a, b) at similar magnitude as the ST4 model results (Figs. 2a–d and 3 a–d), but instead of keep increasing for higher winds as shown by the ST4 results, $\frac{EF_c}{\rho_{air}|U_{10}|^3}$ decreases with wind for the ST6 results. More interestingly, when normalized by u_*, there is a clear separation in the behavior of $\frac{EF_c}{\rho_{air}|u_*|^3}$ between 10 ms^{-1} wind and other wind speeds that are all collapsed together and at a much higher level.

While the ratio of EF_c relative to EF_{air} varies from 82% to 100% with time for all wind speeds (Fig. 8e), its variation with fetch is much smaller with all wind speed collapsed together around 95% except for 10 ms^{-1} wind (Fig. 7e). This different behavior between fetch and duration limited experiments is more profound when the ratio is plotted against wave age (Figs. 7f and 8f), similar to what we observed in the ST4 results. Note, the ratio in the duration dependent experiments is much smaller than the ST4 cases for wave age less than 15 indicating more active breaking of young waves.

5.2. Moving TC experiments

The distribution of the wave age in the ST6 experiments (Fig. 9a) looks similar to the ST4 cases but with much smoother spatial gradient (i.e. the variation of wave age with distance from the storm center is much smaller). Like the ST4 cases, the spatial distribution of the normalized KE flux $\frac{EF_c}{\rho_{air}|u_*|^3}$ (Fig. 9b) roughly follows the spatial distribution of input wave age and increases towards the periphery, but its magnitude is much higher than the ST4 cases. This is mainly because the friction velocity calculated by the ST6 package is much lower than that calculated by the ST4 package at high winds (Figs. 6 and 10).

The spatial distribution of $\frac{EF_c}{\rho_{air}|u_*|^3}$ is in general similarly to the ST4 results for the slower moving TC, while the structure is strongly distorted for the faster storm. Interestingly, same as what we found in the ST4 cases, both experiments show a large normalized KE flux area wrapped in the small normalized KE flux region right in front of the hurricane center with more profound values for the faster moving storm indicating older waves in this region is giving up energy to the subsurface currents.

The ratio of EF_c vs. EF_{air} also has similar spatial structure as the ST4 case for the 5 ms^{-1} storm, but the reduction is much stronger. While for

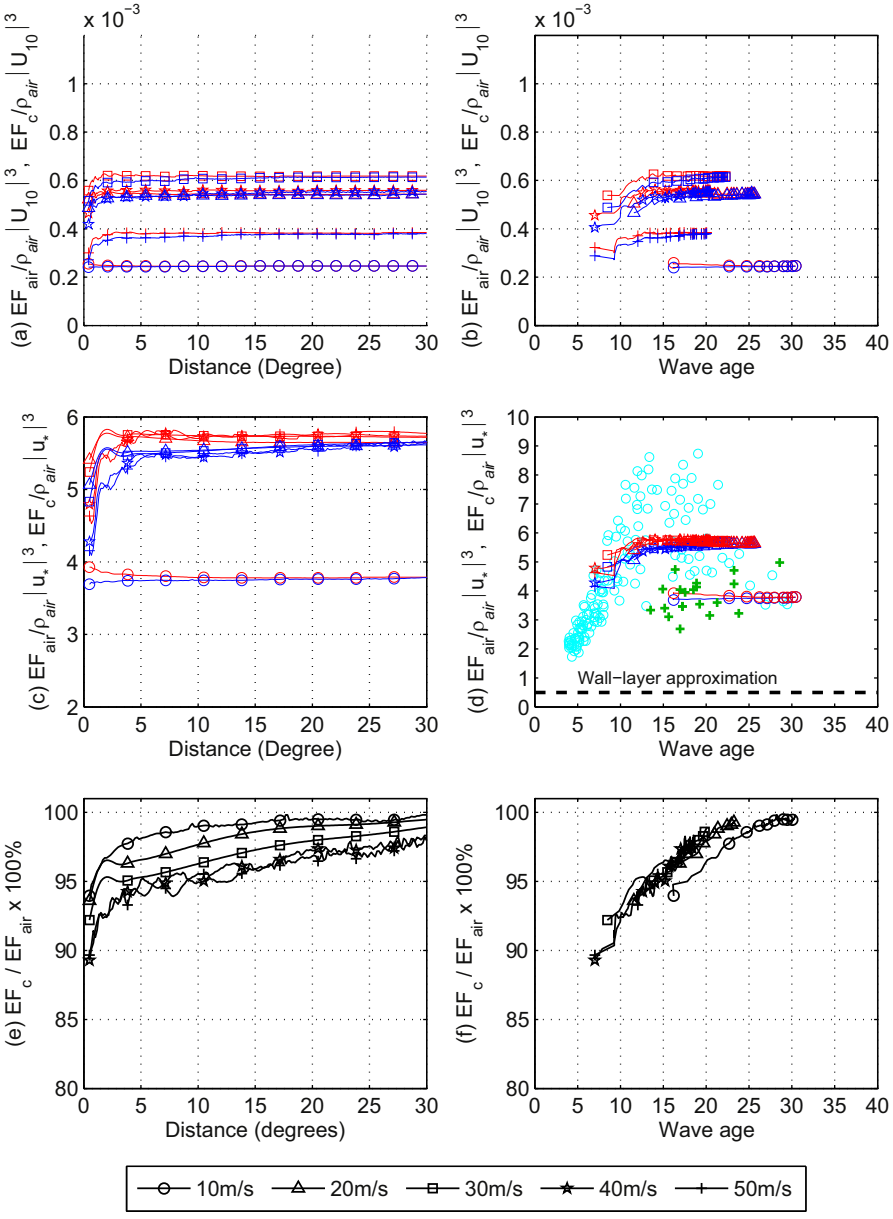

Fig. 7. Same as Fig. 2 except model results are computed using the ST6 source function.

the faster moving storm, most of the study area is covered in dark blue indicating more than 25% of reduction. As shown in the duration dependent experiments, the ratio of EF_c vs. EF_{air} is smaller in ST6 for waves with age less than 15 due to more active breaking of young waves. Since the wave age in the entire study area is smaller than 15 (Fig. 9a), we expect to see more reduction in the KE fluxes.

The scatter plot of $\frac{EF_{air}}{\rho_{air}|u_*|^3}$ and $\frac{EF_c}{\rho_{air}|u_*|^3}$ vs. the wave age are plotted in Fig. 10 in the same way as Fig. 6. Notice the wave age range is much smaller in the ST6 cases, and the u_* is much lower for high winds. The normalized air input is on the upper edge of Terray et al. (1996) for the high winds regime, and turns sharply downward for the low wind regime with a clear separation in pattern, same as we have observed in the uniform wind experiments. The $\frac{EF_c}{\rho_{air}|u_*|^3}$ values are also much higher than the ST4 cases and fits the upper limit of the Hwang and Walsh (2016) estimates, calculated with a spectral slope a = -4.33 as discussed at the end of Section 4.

6. Summary

The effect of surface gravity waves on the kinetic energy (KE) fluxes across the air-sea interface has been investigated in a series of numerical experiments. The wave fields are simulated using the WAVEWATCH III (WWIII) model under uniform and tropical cyclone (TC) wind conditions. An air-sea KE flux budget model is used to estimate the difference between the KE fluxes from air and the fluxes to subsurface currents. The ST4 source package (Ardhuin et al., 2010) is used to calculate the wind input term in WWIII for all experiments. The uniform wind and moving TC experiments are also conducted using the ST6 source function (Babanin, 2011) in WWIII to evaluate the uncertainty of our estimates brought about by different sink and source formulations.

6.1. Uniform wind experiments

The normalized fluxes are very similar between the duration and fetch dependent cases. The normalized KE flux in terms of the 10-m wind speed increases with wind speed being consistent with the analytical expression proposed by Hwang and Sletten (2008), while the normalized KE flux in terms of the wind friction velocity is less dependent on the wind speed. The ratio of EF_c/EF_{air} can be as small as

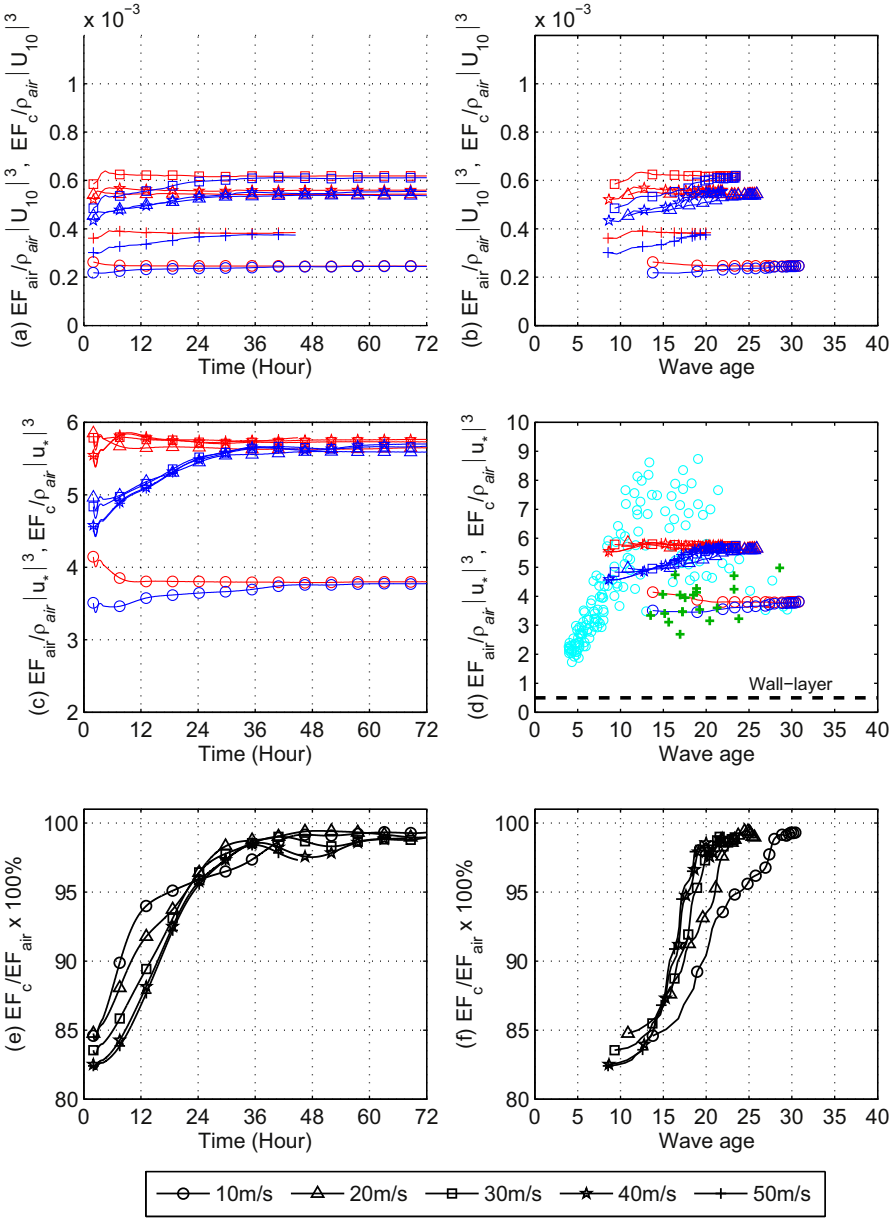

Fig. 8. Same as Fig. 3 except model results are computed using the ST6 source function.

85% for all wind speeds. Another important finding from these simulations is that $\frac{EF_c}{\rho_{air}|u_*|^3}$ is not only a function of the wave age but also increases with wind speed at wave age greater than 15.

While both the ST6 and ST4 results show different behavior in the ratio of EF_c/EF_{air} between fetch and duration limited experiments indicating different growth rate for fetch and duration in the model, the normalized KE fluxes are very different between the two with $\frac{EF_c}{\rho_{air}|u_*|^3}$ given by ST6 features a clear separation between 10 ms^{-1} wind and other wind speeds that are all collapsed together and at a much higher level. This exercise has illustrated the important effect of source function on KE flux estimates. While different source functions can provide similar bulk wave parameters that are well validated against observations, the KE fluxes calculated by these sources functions can be very different.

6.2. TC experiments

The ST4 source package is used for all TC experiments. For stationary TCs, the ratios of EF_c to EF_{air} are reduced to less than 80% within the radius of maximum wind (RMW), and increase roughly quadratically with radius outside the eye wall. The reduction is insensitive to the change of the RMW, but is enhanced with increasing MWS. When a TC moves, the wave field becomes asymmetric with higher and longer waves in the front-right quadrant of the TC and lower and shorter waves in the rear-left quadrant. The asymmetry of the wave field further reduces the KE flux into subsurface currents in the rear-right quadrant of the TC. For a TC with MWS equal to 45 ms^{-1}, the KE flux into subsurface currents can be less than 85% of the air input in the right front quadrant of the storm. Although the dependence of the normalized KE flux on the input wave age is qualitatively similar to that found in the uniform wind experiments, it scatters more widely due to the complexity of the wave field under TC conditions. Furthermore, the waves generated near the eye wall of a faster moving TC can give up energy to the subsurface currents when they decay farther away from the storm center in the left rear quadrant of the storm.

ST6 source package gives much higher $\frac{EF_{air}}{\rho_{air}|u_*|^3}$ and $\frac{EF_c}{\rho_{air}|u_*|^3}$ due to the fact that it produces much lower u_* than ST4 for high winds. The ratio of EF_c to EF_{air} are also much smaller in the ST6 experiments,

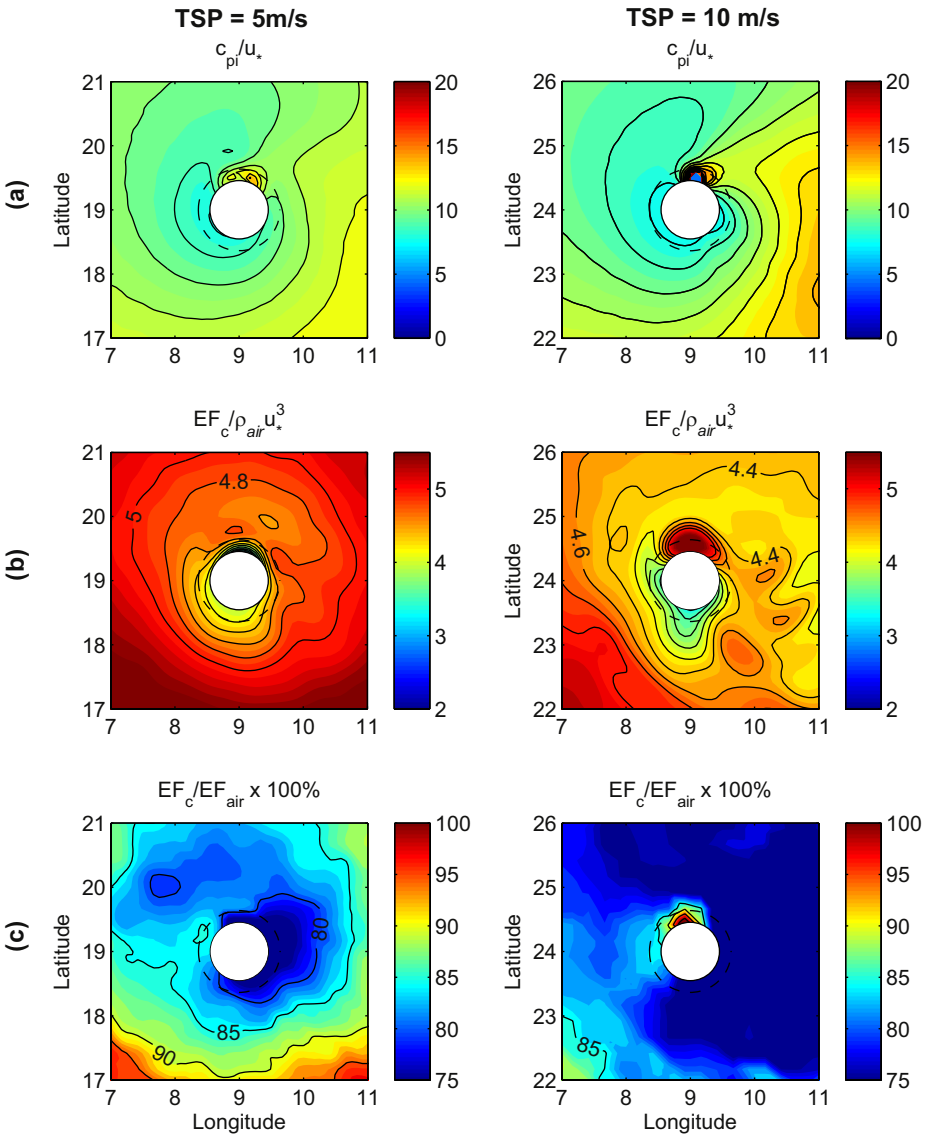

Fig. 9. Same as Fig. 5 except model results are computed using the ST6 source function.

especially for the faster moving storm due to more active breaking of young waves.

All model results for the KE flux are roughly consistent with the previous estimates by Terray et al. (1996) and Drennan et al. (1996) based on observations, although their estimates scatter widely. The model results also agree well with the empirical formulation derived by Hwang and Sletten (2008) and Hwang and Walsh (2016) especially for young waves under high wind conditions.

Liu et al. (2017) compared the performance of ST4 and ST6 together with two other source function packages within the WWIII framework through intensive comparisons with radar altimeter measurements, scanning radar altimeter measurements, and buoy observations during hurricane Ivan in 2004. Model-data comparison statistics (bias, root mean square error, correlation, and scatter index) for significant wave height, mean wave direction and wave period suggest that source packages ST3, ST4 and ST6 perform well for simulating wave parameters under the strong hurricane. It is found that all three packages give some degree of overestimation on crossing and opposing swells, and the choice of drag coefficient cap will influence the well-tuned wave growth behavior under low to moderate winds. However, no conclusion is drawn on the most accurate package among the three due to the uncertainty in the wind forcing.

The results of this study clearly demonstrate that surface gravity waves may play an important role in the air–sea kinetic energy flux budget in tropical cyclones. More importantly, $\frac{EF_c}{\rho_{air}|u_*|^3}$ is not only a function of the wave age but also increases with wind speed at wave age greater than 15. These findings suggest that it may be essential to include the surface wave effects with the explicit air–sea energy flux budget calculations in coupled tropical cyclone–ocean prediction models instead of parameterize the TKE flux using u_* alone.

There are certainly some limitations of this study. Current study is limited to deep water only so that the waves will have no interaction with the bottom, which greatly simplified our budget calculation but our findings may not apply for shallow and intermediate water depth when bottom friction become an important player for dissipation. All calculations are performed using the stand-alone WWIII model. To clarify the physical processes, the condition is simplified such that the wind is not allowed to vary based on the sea state and no ocean currents are considered. However, evolving wind and current fields in realistic weather may result in significant differences in the KE flux ratios. Further modeling and observational studies are needed to clarify the dependence of the KE flux for various wind and wave conditions.

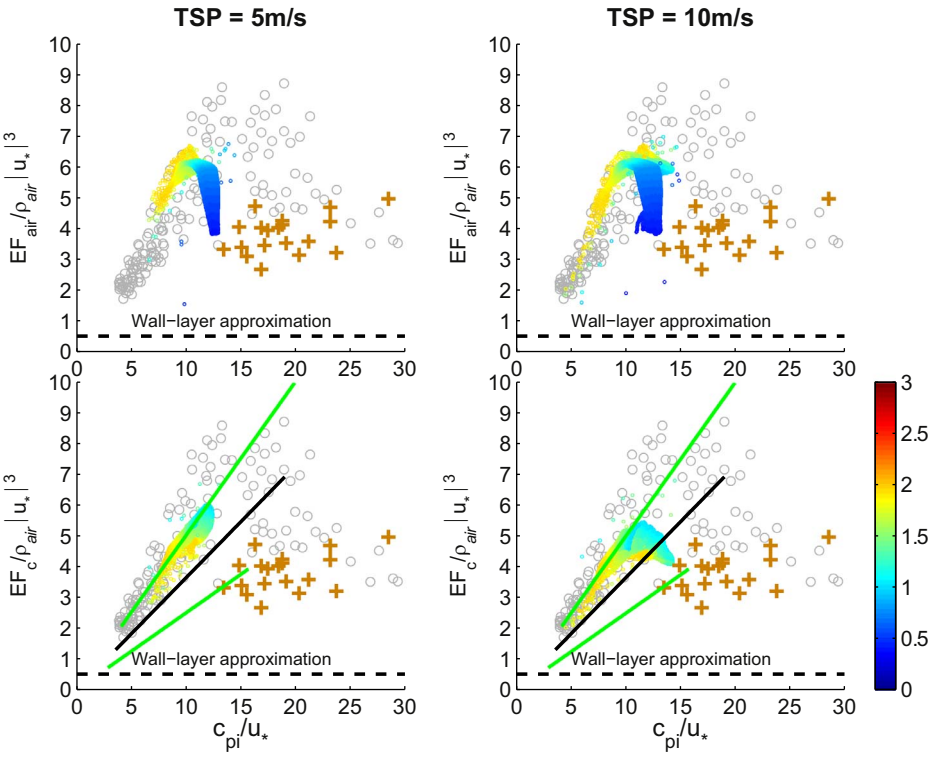

Fig. 10. Same as Fig. 6 except model results are computed using the ST6 source function.

Acknowledgments

The authors would like to express their appreciation to the anonymous reviewers for very helpful comments and suggestions. We thank the WAVEWATCH III®development team for developing the code used in this study. NOAA/NWS/EMC/WAVEWATCH III public release version 4.18 is used to generate the data for this study. This work was funded by the Office of Naval Research under program element 0602435N. This paper is contribution NRL/JA/7320-17-3412 and has been approved for public release.

References

Allard, R., Rogers, E., Martin, P., Jensen, T., Chu, P., Campbell, T., Dykes, J., Smith, T., Choi, J., Gravois, U., 2014. The US navy coupled ocean-wave prediction system. Oceanography 27 (3), 92–103. http://dx.doi.org/10.5670/oceanog.2014.71.

Ardhuin, F., Rogers, W.E., Babanin, A.V., Filipot, J., Magne, R., Roland, A., van der Westhuysen, A., Queffeulou, P., Lefevre, J., Aouf, L., Collard, F., 2010. Semiempirical dissipation source functions for ocean waves. Part I: definition, calibration, and validation. J. Phys. Oceanogr. 40, 1,917–1,941.

Babanin, A.V., Young, I.R., Banner, M.L., 2001. Breaking probabilities for dominant surface waves on water of finite constant depth. J. Geophys. Res. 106 (C6), 11659–11676.

Babanin, A.V., Chalikov, D., Young, I.R., Savelyev, I., 2007a. Predicting the breaking onset of surface water waves. Geophys. Res. Lett. 34, L07605. http://dx.doi.org/10.1029/2006GL029135.

Babanin, A.V., Banner, M.L., Young, I.R., Donelan, M.A., 2007b. Wave follower measurements of the wind input spectral function. Part 3. Parameterization of the wind input enhancement due to wave breaking. J. Phys. Oceanogr. 37, 2764–2775.

Babanin, A.V., 2011. Breaking and Dissipation of Ocean Surface Waves. Cambridge University Press.

Banner, M.L., Young, I.R., 1994. Modeling spectral dissipation in the evolution of wind waves. Part I: assessment of existing model performance. J. Phys. Oceanogr. 24, 1550–1571.

Banner, M.L., Babanin, A.V., Young, I.R., 2000. Breaking probability for dominant waves on the sea surface. J. Phys. Oceanogr. 30, 3145–3160.

Banner, M.L., Gemmrich, J.R., Farmer, D.M., 2002. Multiscale measurements of ocean wave breaking probability. J. Phys. Oceanogr. 32, 3364–3375.

Banner, M.L., Morison, R.P., 2010. Refined source terms in wind wave models with explicit wave breaking prediction. Part I: Model framework and validation against field data. Ocean Modell. 33, 177–189.

Bidlot, J.-R., Abdalla, S., Janssen, P., 2005. A Revised Formulation For Ocean Wave Dissipation in CY25R1. ECMWF, Reading, United Kingdom, pp. 35 Research Dept. Tech. Rep. Memo. R60.9/JB/0516.

Bidlot, J.-R., Janssen, P., Abdalla, S., 2007. A Revised Formulation of Ocean Wave Dissipation and its Model Impact. ECMWF, Reading, United Kingdom, pp. 27 Tech. Rep. Memo. 509.

Birch, K.G., Ewing, J.A., 1986. Observations of Wind Waves on a Reservoir. Institute of Oceanographic Sciences, Wormley, UK, pp. 37 Report 234.

Booij, N., Ris, R.C., Holthuijsen, L.H., 1999. 1999. A third-generation wave model for coastal regions, part 1: model description and validation. J. Geophys. Res. 104 (C4), 7649–7666.

Cavaleri, L., 2009. Wave modeling – missing the peaks. J. Phys. Oceanogr. 39, 2757–2778. http://dx.doi.org/10.1175/2009JPO4067.1.

Curcic, M., Chen, S.S., Özgökmen, T.M., 2016. Hurricane-induced ocean waves and Stokes drift and their impacts on surface transport and dispersion in the Gulf of Mexico. Geophys. Res. Lett. 43, 2773–2781. http://dx.doi.org/10.1002/2015GL067619.

Chen, S.S., Zhao, W., Donelan, M.A., Price, J.F., Walsh, E.J., 2007. The CBLAST-hurricane program and the next-generation fully coupled atmosphere–wave–ocean models for hurricane research and prediction. Bull. Amer. Meteor. Soc. 88, 311–317.

Chen, S.S., Zhao, W., Donelan, M.A., Tolman, H.L., 2013. Directional wind-wave coupling in fully coupled atmosphere-wave-ocean models: results from CBLAST-Hurricane. J. Atmos. Sci. 70, 3198–3215. http://dx.doi.org/10.1175/JAS-D-12-0157.1.

Chen, S.S., Curcic, M., 2016. Ocean surface waves in Hurricane Ike (2008) and Superstorm Sandy (2012): coupled modeling and observations. Ocean Modell. 103, 161–176. http://dx.doi.org/10.1016/j.ocemod.2015.08.005.

Csanady, G.T., 2001. Air-Sea Interaction Laws and Mechanisms. Cambridge University Press Section 1.4.3 15-17.

Donelan, M.A., Hamilton, J., Hui, W.H., 1985. Directional spectra of wind generated waves. Philos. Trans. R. Soc. London Ser. A 315, 509–562.

Donelan, M.A., Pierson, W., 1987. Radar scattering and equilibrium ranges in wind-generated waves with application to scatterometry. J. Geophys. Res. 92 (c5), 4971–5029.

Donelan, M.A., Shafel, M., Graber, H., Liu, P., Schwab, D., Venkatesh, S., 1992. On the growth rate of wind-generated waves. Atmos.–Ocean 30, 457–478.

Donelan, M.A., Drennan, W.M., Kasaros, K.B., 1997. The air-sea momentum flux in conditions of wind sea and swell. J. Phys. Oceanogr. 27, 2087–2099.

Donelan, M.A., Haus, B.K., Reul, N., Plant, W.J., Stiassnie, M., Graber, H.C., Brown, O.B., Saltzman, E.S., 2004. On the limiting aerodynamic roughness of the ocean in very strong winds. Geophys. Res. Lett. 31, L18306. http://dx.doi.org/10.1029/2004GL019460.

Donelan, M.A., Babanin, A.V., Young, I.R., Banner, M.L., 2006. Wave-follower field measurements of the wind-input spectral function. part ii: parameterization of the wind input. J. Phys. Oceanogr. 36 (8), 1672–1689.

Donelan, M.A., Curcic, M., Chen, S.S., Magnusson, A.K., 2012. Modeling waves and wind stress. J. Geophys. Res. Oceans 117, C00J23. http://dx.doi.org/10.1029/2011JC007787.

Drennan, W.M., Donelan, M.A., Terray, E.A., Katsaros, K.B., 1996. Oceanic turbulence dissipation measurements in SWADE. J. Phys. Oceanogr. 26, 808–815.

Fan, Y., Ginis, I., Hara, T., 2009a. The effect of wind-wave-current interaction on air-sea momentum flux and ocean response in tropical cyclones. J. Phys. Oceanogr. 39, 1019–1034. http://dx.doi.org/10.1175/2008JPO4066.1.

Fan, Y., Ginis, I., Hara, T., Wright, W., Walsh, E., 2009b. Numerical simulations and observations of the surface wave fields under an extreme tropical cyclone. J. Phys. Oceanogr. 39, 2097–2116.
Fan, Y., Ginis, I., Hara, T., 2010. Momentum flux budget across the air-sea interface under uniform and tropical cyclone winds. J. Phys. Oceanogr 40, 2221–2242. http://dx.doi.org/10.1175/2010JPO4299.1.
Fan, Y., Rogers, W.E., 2016. Drag coefficient comparisons between observed and model simulated directional wave spectra under hurricane conditions. Ocean Modeling 102, 1–13. http://dx.doi.org/10.1016/j.ocemod.2016.04.004.
Harris, D.L., 1966. The wave-driven wind. J. Atmos. Sci. 23, 688–693.
Hasselmann, K., Barnett, T.P., Bouws, E., Carlson, H., Cartwright, D.E., Enke, K., Ewing, J.A., Gienapp, H., Hasselmann, D.E., Kruseman, P., Meerburg, A., Muller, P., Olbers, D.J., Richter, K., Sell, W., Walden, H., 1973. Measurements of wind-wave growth and swell decay during the Joint North Sea Wave Project (JONSWAP). *Ergänzungsheft zur Deutsch. Hydrogr.* Z. 12, 1–95.
Hasselmann, 1974. On the spectral dissipation of ocean waves due to white capping. Bound.-Layer Meteor. 6, 107–127.
Hasselmann, S., et al., 1988. The WAM model—a third-generation ocean wave pre- diction model. J. Phys. Oceanogr. 18, 1775–1810. http://dx.doi.org/10.1175/1520-0485(1988)018.
Holland, G.J., 1980. An analytic model of the wind and pressure profiles in hurricanes. Mon. Wea. Rev. 108, 1212–1218.
Hwang, A.P., Sletten, M.A., 2008. Energy dissipation of wind-generated waves and whitecap coverage. J. Geophys. Res. 113, C02012. http://dx.doi.org/10.1029/2007JC004277.
Hwang, A., 2016. Fetch- and duration-limited nature of surface wave growth inside tropical cyclones: With applications to air-sea exchange and remote sensing. J. Phys. Oceanogr. 46, 41–56. http://dx.doi.org/10.1175/JPO-D-15-0173.1.
Hwang, A.P., Walsh, E.J., 2016. Azimuthal and radial variation of wind-generated surface waves inside tropical cyclones. J. Phys. Oceanogr. 46. http://dx.doi.org/10.1175/JPO-D-16-0051.1.
Hwang, P.A., Fan, Y., 2017. Effective fetch and duration of tropical cyclone wind fields estimated from simultaneous wind and wave measurements: surface wave and air-sea exchange computation. J. Phys. Oceanogr. 47, 447–470. http://dx.doi.org/10.1175/JPO-D-16-0180.1.
Hwang, P.A., Fan, Y., Ocampo-Torres, F.J., García-Nava, H., 2017. Ocean surface wave spectra inside tropical cyclones. J. Phys. Oceanogr. http://dx.doi.org/10.1175/JPO-D-17-0066.1. (in press).
Janssen, P.A.E.M., 1991. Quasi-linear theory of wind wave generation applied to wave forecasting. J. Phys. Oceanogr. 21, 1631–1642.
Janssen, P., 2004. The Interaction of Ocean Waves and Wind. Cambridge University Press.
Jenkins, A.D., 1987. A Lagrangian model for wind- and wave-induced flux of near-surface currents. Coastal Engineering 11, 513–526.
Kahma, K.K., 1981. A study of the growth of the wave spectrum with fetch. J. Phys. Oceanogr. 11, 1503–1515.
Komen, G.J., Hasselmann S. and Hasselmann, K., 1984. On the existence of a fully developed wind-sea spectrum. J. Phys. Oceanogr. 14, 1,271–1,285.
Liu, B., Liu, H., Xie, L., Guan, C., Zhao, D., 2011. A coupled atmosphere–wave–ocean modeling system: simulation of the intensity of an idealized tropical cyclone. Mon. Wea. Rev. 139, 132–152. http://dx.doi.org/10.1175/2010MWR3396.1.
Liu, Q., Babanin, A., Fan, Y., Zieger, S., Guan, C., Moon, I.-I., 2017. Numerical simulations of ocean surface waves under hurricane conditions: assessment of existing model performance. Ocean Modell. 118, 73–93.
Mellor, G.L., Yamada, T., 1982. Development of a turbulent closure models for planetary boundary layers. J. Atmos. Sci. 31, 1791–1806.
Moon, I.-J., Ginis, I., Hara, T., Tolman, H., Wright, C.W., Walsh, E.J., 2003. Numerical simulation of sea-surface directional wave spectra under hurricane wind forcing. J. Phys. Oceanogr. 33, 1680–1706.
Moon, I.-J., Ginis, I., Hara, T., 2004. Effect of surface waves on air-sea momentum exchange, Part II: behavior of drag coefficient under tropical cyclones. J. Atmos. Sci. 61, 2334–2348.
Noh, Y., Kim, H.J., 1999. Simulations of temperature and turbulence structure of the oceanic boundary layer with the improved near-surface process. J. Geophys. Res. 104 (C7), 15,621–15,634.
Peirson, W.L., Garcia, A.W., 2008. On the wind-induced growth of slow water waves of finite steepness. J. Fluid Mech. 608, 243–274.
Phadke, A.C., Martino, C.D., Cheung, K.F., Houston, S.H., 2003. Modeling of tropical cyclone winds and waves for emergency management. Ocean Eng. 30, 553–578.
Phillips, O.M., 1985. Spectral and statistical properties of the equilibrium range in wind-generated gravity waves. J. Fluid Mech. 156, 505–531.
Powell, M.D., Vickery, P.J., Reinhold, T.A., 2003. Reduced drag coefficient for high wind speeds in tropical cyclones. Nature 422, 279–283.
Rogers, E.W., Babanin, A.V., Wang, D.W., 2012. Observation-consistent input and whitecapping dissipation in a model for wind-generated surface waves: description and simple calculations. J. Atmos. Oceanic Technol. 29 (9), 1329–1346.
Smith, T.A., S. Chen, T. Campbell, P. Martin, W.E. Rogers, S. Gabersek, D. Wang, S. Carroll, and R. Allard, 2013: Ocean-wave coupled modeling in COAMPS-TC: a study of Hurricane Ivan (2004).
Takagaki, N., et al., 2012. Strong correlation between the drag coefficient and the shape of the wind sea spectrum over a broad range of wind speeds. Geophys. Res. Lett. http://dx.doi.org/10.1029/2012GL053988.
Takagaki, N., Komori, S., Suzuki, N., 2016a. Estimation of friction velocity from the wind-wave spectrum at extremely high wind speeds. In: IOP Conference Series: Earth and Environmental Science, . http://dx.doi.org/10.1088/1755-1315/35/1/012009.
Takagaki, N., Komori, S., Suzuki, N., Iwano, K., Kurose, R., 2016b. Mechanism of drag coefficient saturation at strong wind speeds. Geophys. Res. Lett. http://dx.doi.org/10.1002/2016GL070666.
Terray, E.A., Donelan, M.A., Agrawal, Y.C., Drennan, W.M., Kahma, K.K., Willians III, A.J., Hwang, P.A., Kitaigorodskii, S.A., 1996. Estimates of kinetic energy dissipation under breaking waves. J. Phys. Oceanogr. 26, 792–807.
Tolman, H.L., Chalikov, D., 1996. Source terms in a third-generation wind wave model. J. Phys. Oceanogr. 26, 2497–2518.
Tolman, H.L., 1998. Validation of a new global wave forecast system at NCEP. In: Edge, B.L., Helmsley, J.M. (Eds.), Ocean Wave Measurements and Analysis. ASCE, pp. 777–786.
Tolman, H.L., Banner, M., Kaihatu, J., 2013. The NOPP operational wave model improvement project. Ocean Modell. 70, 2–10.
Tolman, H.L., WAVEWATCHIII development group, 2014. User manual and system documentation of WAVEWATCH III version® 4.18(http://polar.ncep.noaa.gov/waves/wavewatch/manual.v4.18.pdf).
Weller, R.A., Donelan, M.A., Briscoe, M.G., Huang, N.E., 1991. Riding the crest: a tale of two wave experiments. Bull. Amer. Meteor. Soc. 72, 163–183.
Wu, J., 1975. Wind-induced drift currents. J. Fluid Mech. 68, 49–70.
Xu, F., Perrie, W., Toulany, B., Smith, P.C., 2007. Wind-generated waves in hurricane Juan. Ocean Mod. 16, 188–205. http://dx.doi.org/10.1016/j.ocemod.20 06.09.0 01.
Young, I.R., 1988. Parametric hurricane wave prediction model. J. Waterw. Port Coastal Ocean Eng. 114, 637–652. http://dx.doi.org/10.1061/(ASCE)0733-950X(1988)114:5(637).
Young, I.R., 1998. Observations of the spectra of hurricane generated waves. Ocean Eng. 25, 261–276. http://dx.doi.org/10.1016/S0029-8018(97)00011-5.
Young, I.R., 2003. A review of the sea state generated by hurricanes. Mar. Struct. 16, 201–218. http://dx.doi.org/10.1016/S0951-8339(02)00054-0.
Young, I.R., 2006. Directional spectra of hurricane wind waves. J. Geophys. Res. 111, C08020. http://dx.doi.org/10.1029/2006JC003540.
Young, I.R., Vinoth, J., 2013. An "extended fetch" model for the spatial distribution of tropical cyclone wind–waves as observed by altimeter. Ocean Eng. 70, 14–24. http://dx.doi.org/10.1016/j.oceaneng.2013.05.015.
Zieger, S., Babanin, A.V., Rogers, W.E., Young, I.R., 2015. Observation based source terms in the third-generation wave model WAVEWATCH. Ocean Modell. 96, 2–25.